International Journal of Automotive Technology, Vol. 23, No. 5, pp. 1185–1195 (2022)
DOI 10.1007/s12239–022–0105–z

pISSN 1229–9138/ eISSN 1976–3832

ACOUSTIC CHARACTERISTICS OF THE ABNORMAL COMBUSTION IN A HIGH-COMPRESSION RATIO, SPARK-IGNITION ENGINE

Junghwan Kim*

School of Energy Systems Engineering, Chung-Ang University, Seoul 06974 Korea

(Received 6 January 2022; Revised 3 March 2022; Accepted 7 March 2022)

ABSTRACT–Engine knocking is often identified by an operator based on the combustion sound emanating from the cylinder block during engine calibration in a test cell. Such human-hearing-based acoustic knock determination is considered the most reliable real-time knock-monitoring method, and it is necessary for selecting an accurate spark timing. In this study, the characteristics of this combustion sound were investigated. To this end, a normal engine calibration experiment was conducted. The engine sound was recorded under various operating conditions by using a copper tube attached to the cylinder block and the microphone of a smartphone. The measured signals were subjected to acoustic analyses, including Fast Fourier transform, smoothing, spectral analysis, and autocorrelation, to compare the sounds recorded at the knock borderline with those recorded in the cases with significantly advanced spark timing. The results of these analyses revealed several features that distinguished the knock sound from the normal combustion sound. The knock sound exhibited distinctions in a high-frequency band between 6,000 and 8,000 Hz. These features can be used to develop effective knock classification models.

KEY WORDS : Engine knocking, Combustion sound, Spectral analysis, Autocorrelation

NOMENCLATURE

KBL	: knock borderline
ECU	: engine control unit
BMEP	: brake mean effective pressure
CA	: crank angle
aTDC	: after top-dead center
RMS	: root mean square
FFT	: fast fourier transform
ACF	: auto-correlation function

1. INTRODUCTION

Engine knocking is a limiting factor in the improvement of spark-ignition engine efficiency (Kalghatgi, 2018). Many approaches, including higher compression ratios, higher octane-rating fuels, various valve timings, and various fuel-injection strategies, have been adopted to improve engine performance and fuel economy (Xu *et al*., 2020). However, none of these approaches have been able to eliminate engine knocking. Spark advance is likely limited to the point at which the first knock cycle is observed and is thus called the knock borderline (KBL) spark timing. Under most operating conditions, engine knocking starts to occur before the spark timing reaches the maximum brake torque timing. Therefore, it is critical to detect engine knocking and quantify its intensity to maximize the spark advance while avoiding knocking (Peyton Jones *et al*., 2014). KBL timings based on inaccurate knock determination either deteriorate fuel economy or cause engine hardware failure.

Many knock determination and quantification methods are based on individual in-cylinder pressure traces (Wang *et al*., 2017). Although they are not as direct as optical monitoring data, the in-cylinder pressure data provide reliable information when measured over consecutive engine cycles. Due to the randomness of knock, it has been recommended that the in-cylinder pressure traces of 1,000 engine cycles be acquired at a crank angle resolution of 0.2° to accurately determine knock intensity (Brunt *et al*., 1998). Moreover, in-cylinder pressure measurements can capture super-knock events (Liu *et al*., 2019). The signal processing of individual in-cylinder pressure data is vital in combustion diagnostics (Maurya *et al*., 2013). Hamilton and Cowart (2008) applied a bandpass filter with a normalized frequency band between 0.2 and 0.8 into the pressure trace for knock intensity calculation. Lee *et al*. (1998) developed a knock determination method based on the knock intensity estimated using in-cylinder pressure data. Their method involved conducting a non-dimensional analysis to determine the threshold knock intensity applicable under all operating conditions. Based on the results of a cross-correlation analysis of multiple engine cylinders, Leppard (1982) concluded that the occurrence

**Corresponding author*. e-mail: jkim77@cau.ac.kr

and intensity of knock depend only on the individual cylinder conditions.

The use of high-speed thermocouples and ion probes for in-cylinder measurement provides an improved understanding of knock occurrence and locations. Cho *et al*. (2018) investigated the in-cylinder temperature distribution and flame development direction by using thermocouples and ion probes attached to the engine head and head gasket. Their experimental results indicated that knock occurred at the intake side, where the flame propagation speed was the highest. Abu-Qudais (1996) demonstrated a potential knock detection method based on exhaust gas temperature. The decrease in exhaust gas temperature is proportional to the spark advance until the occurrence of knock. Therefore, in their method, knock was considered to occur at the point where the decrease in exhaust temperature was significantly enlarged.

Meanwhile, the use of engine block vibration for knock detection has been explored. An accelerometer attached to the engine block can absorb the vibration transmitted from the cylinders. The excellent durability and cost-effectiveness of accelerometers makes them suitable for use as knock sensors in spark-ignition engines. Moreover, accelerometer signals recorded using a high-speed data acquisition system can even be used to determine in-cylinder pressure (Bennett *et al*., 2017). Ettefagh *et al*. (2008) developed a knock detection method based on an autoregressive moving-average parametric model that used the cylinder block vibration data measured with an accelerometer. Furthermore, a deflation method was used as an effective blind source-separation technique to distinguish among the various vibration sources in internal combustion engine vibration signals (Liu *et al*., 2008).

Despite the above-described diverse efforts toward the development of knock detection techniques by using a variety of sensors, most engine developers continue to rely on audible knock for spark timing calibration. Engine operators advance the spark timing until they hear pinging sounds and repeat this process at all other operating points.

The spark timing that provides the first pinging sound is considered the KBL timing. Metal tubing is often used to deliver the pinging sound to an operator sitting outside the engine operating room. The tube not only delivers the engine sound but also isolates it from noise. Therefore, it is critical to characterize the engine sound delivered through the tube to objectify knock judgements based on audibility (Novella *et al*., 2022). However, to the best of our knowledge, this sound has not been acoustically analyzed thus far. Yun and Lee (2017) developed the evaluation methods for the diesel engine knock sound based on the degree of modulation. The method was validated with numerically synthesized combustion sound signals. The present study investigates the characteristics of the knock sound measured in the same manner as in an actual engine calibration test. The sound signals are acquired when setting the spark timing at the KBL and other substantially advanced timings to compare the sounds under normal operation conditions with those under severe knocking. The distinctive features of the knock sound vis a vis those of normal operation sounds can contribute to development of sound-based knock classification model using machine learning algorithms.

2. INSTRUMENTATION

A four-cylinder, port-fuel-injection, naturally aspirated, spark-ignition engine was prepared for use in the engine experiments. The geometrical compression ratio of the experimental engine was 14. A variable valve timing system was installed on both the intake and exhaust camshafts. The details of the engine specifications are listed in Table 1. An eddy-current-type dynamometer was coupled with the engine for loading. As the engine rotates, the dynamometer generates an eddy current. Because the eddy current induces a force in the direction opposite to the engine rotation, it reduces the engine speed (PowerLink, 2020). The torque generated by the engine balances the eddy current and thus maintains the desired engine speed. Since the eddy current is generated only when the engine rotates, an additional motoring device is required to initiate the engine rotation. A 12-V battery-operated stock starter motor was used to start the engine. When an appropriate engine speed was reached, fuel was injected, and then, a spark was applied to ignite fuel in the cylinder. A stock flywheel for a manual transmission was installed at the front of the engine for balancing.

In this study, regular gasoline with the research octane number range of 91 ~ 93, which is sold in all gas stations in South Korea, was used.

An external cooling system was used to control the engine coolant temperature. The cooling system monitored the coolant temperature at the engine inlet and maintained the fluid at desired temperature by passing it through a water-cooling heat exchanger. The stock thermostat was disabled to facilitate consistent flow of the coolant fluid through the coolant temperature control system. The coolant

Table 1. Engine specifications.

Parameters	Units	Nominal values
Number of cylinders	-	4
Ignition type	-	Spark ignition
Displacement	cm^3	1,368
Bore	mm	72
Stroke	mm	84
Fuel supply	-	Port injection

was heated to expedite engine warmup before starting by using an electric heater installed in the external cooling system.

An ETAS ETK engine control unit (ECU) was employed for engine operation. The parametric tables of all of the operating parameters were stored in the ECU. Specific values based on a given engine speed and torque were pulled from the corresponding tables. The values stored in the tables were used by default, unless the operator overrode them. In the present study, only the spark timing was adjusted, while all of the other parameters were set using the tables. The ECU was capable of adjusting the spark timing of individual cylinders.

2.1. Measurement Devices

Four piezoelectric pressure transducers (6056A, Kistler, Switzerland) were used to measure the in-cylinder pressures with a high sampling rate. An encoder (Type 2614C11, Kistler, Switzerland) installed on the crankshaft recorded five samples per degree of crank angle, which was equivalent to 60 kHz at an engine speed of 2,000 rev/min. The in-cylinder pressure traces of 300 consecutive cycles were acquired using an AVL data-acquisition system (Indicom, AVL, Austria). The measured in-cylinder pressure signals were post-processed and used for high-quality combustion diagnosis. To this end, a four-step process was used in combination with ad-hoc methods and experience-based logics, as recommended in (Payri *et al*., 2010).

A copper tube was pushed through the bolt head on the engine block near the first cylinder (Cyl-1) as shown in Figure 1. The tube ran through the engine test cell to the control room, where an operator monitored the knock sound. The length of the copper tube was approximately 5 m. A smartphone (Note 9, Samsung, South Korea) was used to record the sound transmitted through the copper tube at a sampling frequency of 48 kHz. Recent smartphones are equipped with microphones capable of capturing high-quality sound in close proximity to the noise source (Glowacz, 2019). At each operating point, the sound was recorded for approximately 1 min. The sound file contained both raw and filtered signals. The raw signal was used because the noise cancellation applied by the microphone suppressed the knock sound.

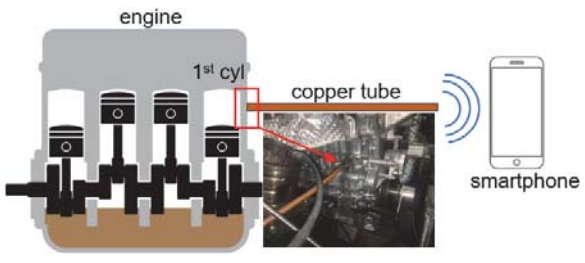

Figure 1. Schematic of combustion sound measurement setup.

Table 2. Operating conditions of the nine runs.

Run number	Point name	Engine speed	BMEP	Adjusted cylinder #	Spark timing
-	-	rev/min	kPa	-	aTDC
1	1500/4	1500	400	-	KBL
2		1500	400	1	-15
3		1500	400	4	-15
4	1500/6	1500	600	-	KBL
5		1500	600	1	-6
6		1500	600	4	-6
7	2000/4	2000	400	-	KBL
8		2000	400	1	-12
9		2000	400	4	-12

2.2. Experimental Procedure

The engine experiment was performed at three different speed and load conditions. At engine speeds of 1,500 rev/min and 2,000 rev/min, Brake mean effective pressure (BMEP) was set at 400 kPa and 600 kPa. These operating conditions were chosen to induce knocking while minimizing the engine damage. At each operating point, three cases were tested. In the first case, the spark timing was set at the KBL. The operator determined the KBL based on the combustion sound from the tube. In the second case, the spark timing of the first cylinder (Cyl-1) was substantially advanced until the knocking was severe, and the spark timings of the other three cylinders were set at the KBL. At 1500/4 point, the Cyl-1 spark timing was advanced to -15 crank angles (CA) after top-dead center (aTDC). Finally, in the third case, the conditions of the second case were replicated for Cyl-4. The operating conditions corresponding to the points and the associated runs are listed in Table 2.

3. RESULTS AND DISCUSSION

The statistics recorded under the three operating conditions used in this study are summarized in Table 3. The KBL cases not only yielded lower maximum values than the advanced spark timing cases but also lower crest factors. The crest factor was computed as the ratio of the peak value to the root mean square (RMS) value, and it indicated how extreme the peak values were in the waveform (Pachaud *et al*., 1997).

Figure 2 presents a comparison of the KBL and severe knock cases for the first operating point. Figures 2 (a) and 2 (b) show the raw and smoothed signals of the two cases, respectively. The Savitzky–Golay filter is a well-known low-pass filter used for data smoothing (Gryllias and Antoniadis, 2013). Figure 2 (c) presents a comparison of

the smoothed signals of the KBL and severe knock cases. The repeated high-amplitude fluctuations in the severe knock cases indicate that knocking occurred consistently. Note that the KBL and severe knock signals in Figure 2 were not obtained simultaneously but in two different runs.

Fast Fourier transform (FFT) was applied to the signals to convert them from the time domain to the discrete frequency domain. Figure 3 shows the frequency-domain power spectrum of the KBL case at the 2000/4 point. Note that 2,000 rev/min is equivalent to 33.3 Hz. The 66 Hz component could have originated from the expansion stroke, which occurred twice per revolution in a 4-cylinder engine. The 133 Hz component could belong to some event that occurred four times per revolution, for example, valve operation. None of the high-frequency components were significant. However, the severe knock case contained high-frequency components at approximately 8 kHz, as shown in Figure 4. Since human ears can detect sounds ranging from 2 to 20 kHz, the 8 kHz components must have been the ticking sounds that the operator identified as the knock sounds. The 66 Hz component was not present in the severe knock case. These results indicate that the severe knock consumed most of the fuel and air mixture, and the main combustion event was substantially weakened.

The spectral analysis was continued to compare the KBL and severe knock cases in their frequency domains. Note that the signal contained only the components between 20 Hz and 20,000 Hz, which is the audible range of human ears. Figures 5 ~ 7 show that a common discrepancy between the two cases was found in the 30% range, which corresponds to 8 kHz. The greater magnitudes at 75 ~ 80 % normalized frequency differed the KBL cases from the severe knock cases at 1500/6 and 2000/4 points. Meanwhile, Figure 5 shows that the severe knock case at 1500/4 point exhibited as greater power spectrum as the KBL case. The power spectra of the severe knock cases consistently contained frequency components higher than the 80 % normalized frequency of 20,000 Hz.

Table 3. Statistics of the KBL and severe knock cases under the three operating conditions.

Run#	Max (V)	Min (V)	Mean (V)	RMS	Dynamic range	Crest factor
1	0.37	-0.37	-2.1E-05	0.051	217	17.3
2	1.02	-1.00	-1.3E-05	0.084	171	21.7
4	0.71	-0.74	-2.1E-05	0.120	174	15.4
5	1.02	-1.04	1.7E-06	0.102	159	20.1
7	0.84	-0.86	-2.5E-05	0.150	145	14.9
8	1.12	-1.07	-1.9E-05	0.113	180	20.0

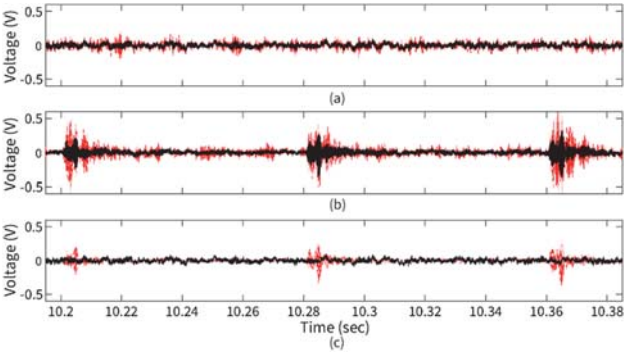

Figure 2. (a) Raw and smoothed signals of the KBL case; (b) Raw and smoothed signals of the severe knock case; (c) Smoothed signals of the KBL and severe knock cases.

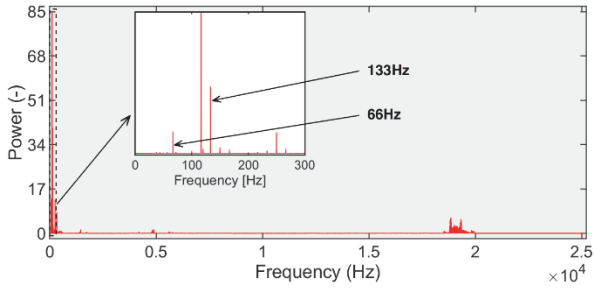

Figure 3. Power spectrum of the 2000/4 KBL case.

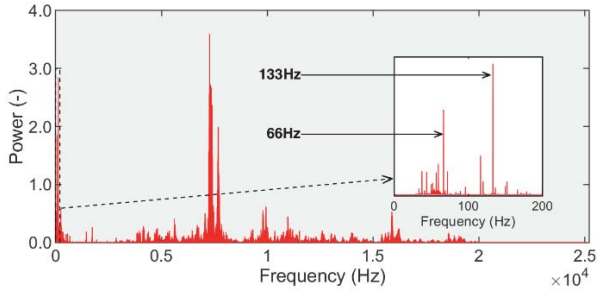

Figure 4. Power spectrum of the 2000/4 severe knock case.

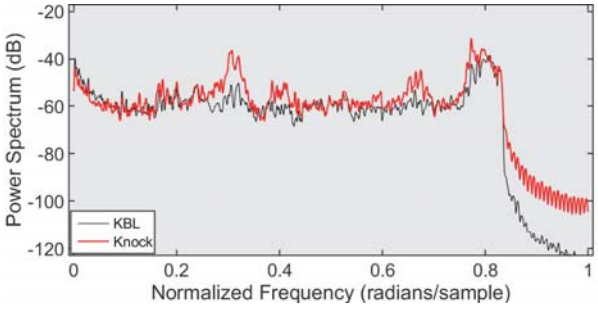

Figure 5. Power spectrum with respect to normalized frequency at the 1500/4 point.

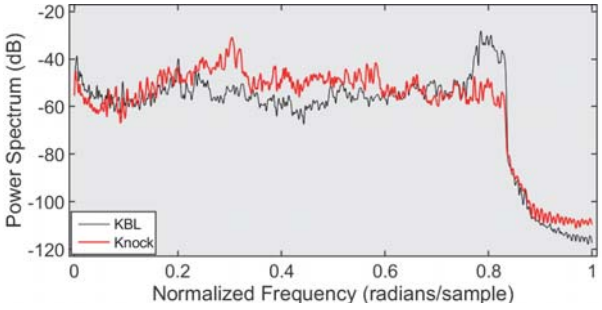

Figure 6. Power spectrum with respect to normalized frequency at the 1500/6 point.

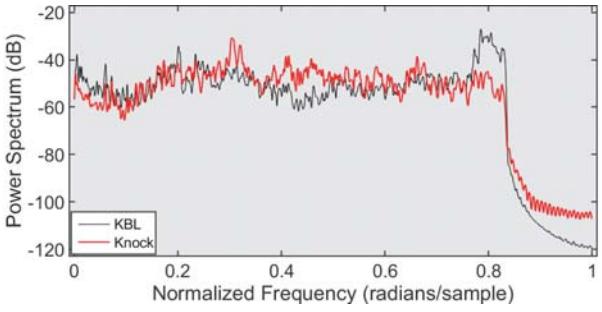

Figure 7. Power spectrum with respect to normalized frequency at the 2000/4 point.

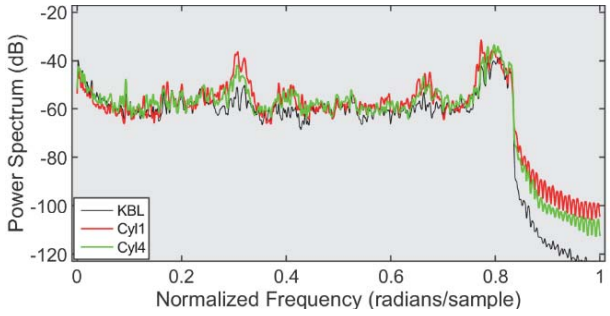

Figure 8. Power spectra of the Cyl-1 and Cyl-4 cases compared to that of the KBL case at the 1500/4 point.

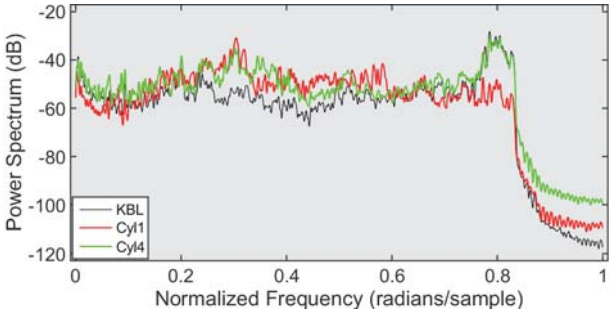

Figure 9. Power spectra of the Cyl-1 and Cyl-4 cases compared to that of the KBL at the 1500/6 point.

Figures 8 ~ 9 show that at the 1500/4 and 1500/6 operating points, respectively, the magnitude of the 30 % frequency component was different in the case of Cyl-1 than that in the case of Cyl-4. In addition, above 80 % frequency, a discrepancy was observed among the three cases. In general, the severe knock cases exhibited higher magnitude, but the difference was not consistent at the two operating points.

Figures 10 ~ 15 show the probability distributions of the KBL and the severe knock cases. The similarity of the probability distributions be used as an effective feature for signal classification (Yang *et al*., 2020). At all three points, the distributions of the severe knock cases were more concentrated than the standard normal distribution. This might have resulted from the consistent high-amplitude fluctuations generated due to knocking. However, the probability distributions of the KBL cases agreed well with the standard normal distribution. This discrepancy in probability distributions between knock and normal combustion was also found in (Peyton Jones *et al*., 2020).

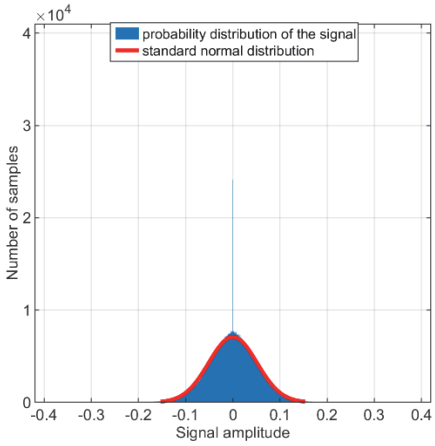

Figure 10. Run#1 KBL at the 1500/4 point.

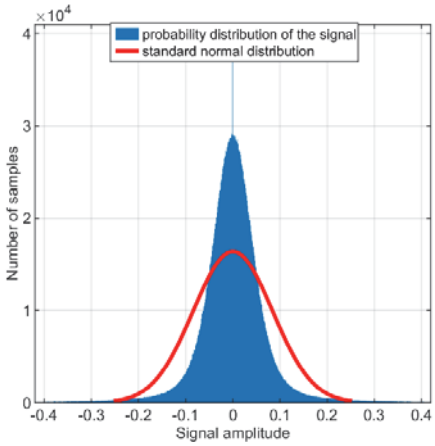

Figure 11. Run#2 severe knock at the 1500/4 point.

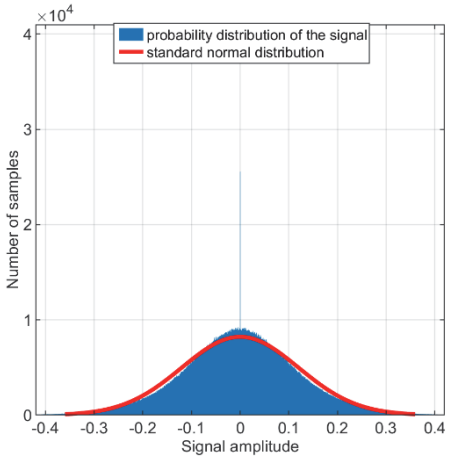

Figure 12. Run#4 KBL at the 1500/6 point.

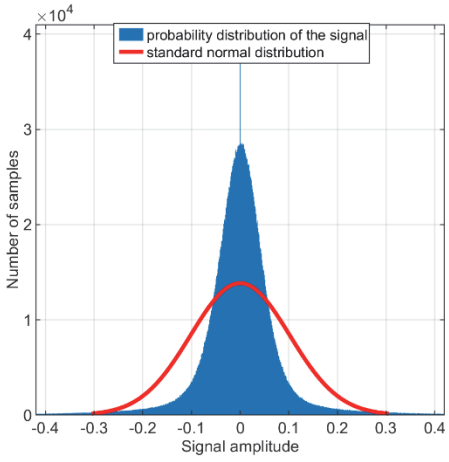

Figure 13. Run#5 severe knock at the 1500/6 point.

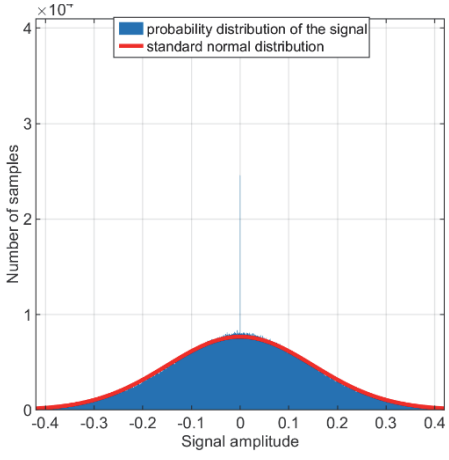

Figure 14. Run#7 KBL at the 2000/4 point.

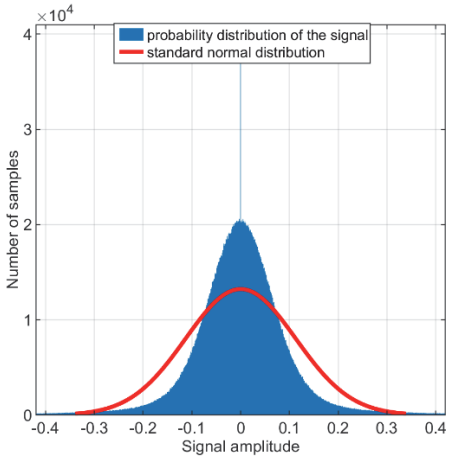

Figure 15. Run#8 severe knock at the 2000/4 point.

Figures 16 ~ 21 show the spectrograms of the KBL and severe knock cases. Each segment contained 1024 samples of the original signal and was overlapped by 50 %, which is a commonly accepted level (Wodecki *et al*., 2019) to achieve a balance between spectral resolution and spectral leakage. All KBL cases exhibited a consistent pattern over the entire sampling period, while the severe knock cases exhibited a somewhat irregular rise and fall in the 5 ~ 8 kHz frequency range. This irregularity was more distinct at the 2000/4 point, indicating that the knock intensity fluctuated. Knocking intensified, as shown in Figure 21. Interestingly, the intensified knocking continued for longer than 0.1 min, which is equivalent to 200 cycles at 2,000 rev/min. In addition, 18 ~ 20 kHz frequency components were elevated up to 50 dB in all KBL cases, which was not exhibited in the severe knock cases.

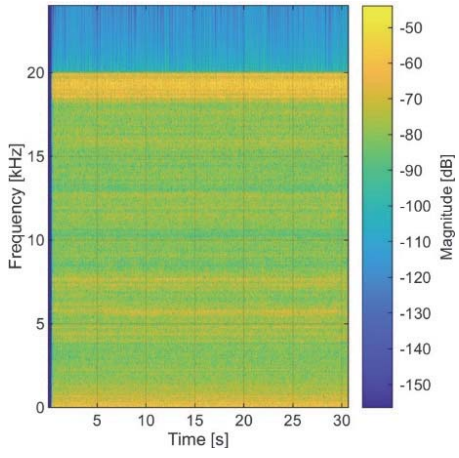

Figure 16. Run#1 KBL at the 1500/4 point.

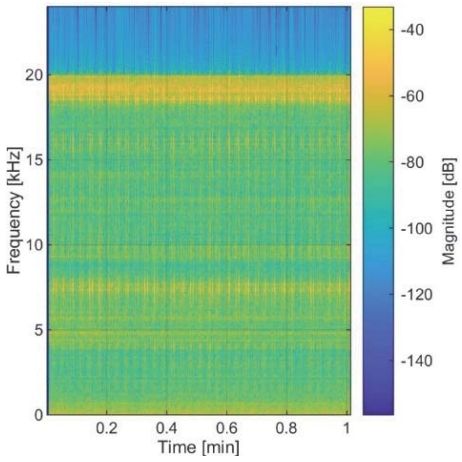

Figure 17. Run#2 severe knock at the 1500/4 point.

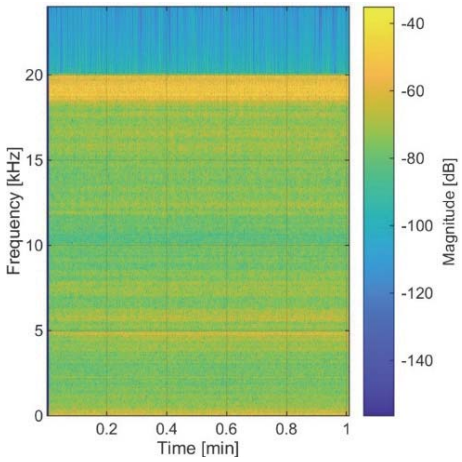

Figure 18. Run#4 KBL at the 1500/6 point.

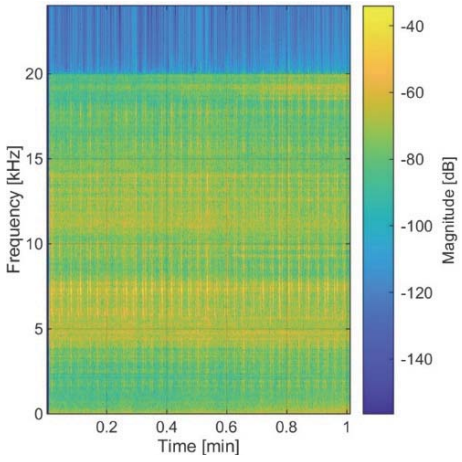

Figure 19. Run#5 severe knock at the 1500/6 point.

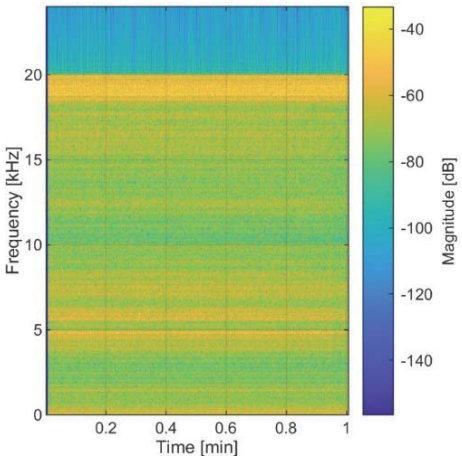

Figure 20. Run#7 KBL at the 2000/4 point.

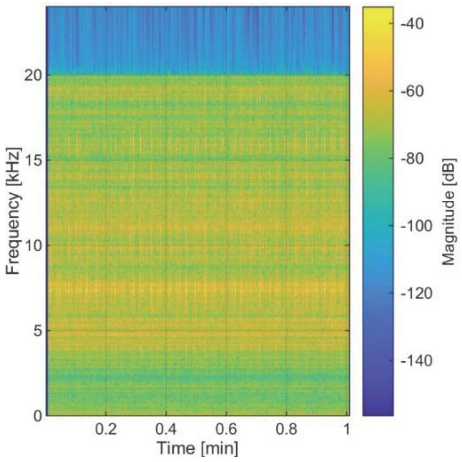

Figure 21. Run#8 severe knock at the 2000/4 point.

The high-frequency components of the acoustic signal were investigated to understand the characteristics of the knock signal. The bandpass filter range was set to 6,000 ~ 8,000 Hz based on the result of the spectral analysis. Figure 22 shows the resulting local maxima of the filtered signals of the KBL and the severe knock cases at the 1500/4 point in the time domain. The high-frequency components were negligible in the KBL case. The high-frequency sound occurred at intervals of 0.080 s, which is equivalent to half of the engine speed, indicating that knocking occurred in most cycles. The amplitude of the high-frequency components gradually increased until it reached a certain threshold; thereafter, it decreased to the lowest level. This pattern was repeated after every four or five cycles.

Figure 23 shows a more detailed shape of the filtered signal of the individual knock cycles shown in Figure 22.

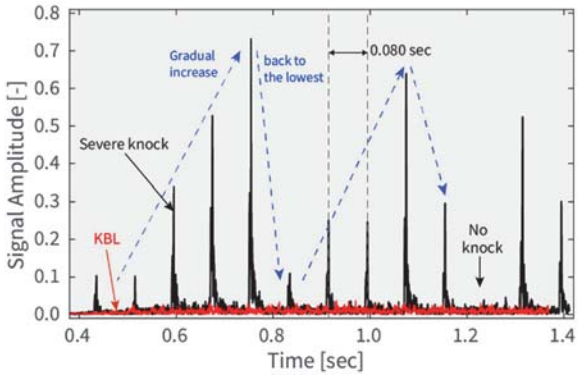

Figure 22. Filtered signals of the KBL and severe knock cases at the 1500/4 point.

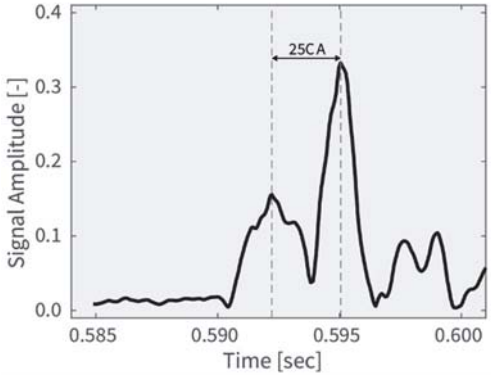

Figure 23. Filtered signal of an individual knock cycle at the 1500/4 point.

The high-frequency sound occurred twice in each knock cycle, as shown in this figure. This two-peak, high-frequency sound was found in most knock cycles. The first high-frequency sound was followed by a stronger second high-frequency sound. The 25CA separation might be too large to consider the two peaks as autoignition of the end gas and subsequent knocking throughout the entire combustion chamber.

Autocorrelation is an effective technique for determining signal characteristics. It has been used in various types of investigations, such as fault diagnosis (Nikula *et al*., 2020). Reliable fault detection features can be extracted by performing autocorrelation analysis (Pichler *et al*., 2016). Su *et al*. (2010) developed a fault diagnosis algorithm for rolling-element bearings based on autocorrelation analysis of vibration signals. Rafiee and Tse (2009) found that the autocorrelation of continuous wavelet coefficients is useful for detecting gear failure.

In this study, similarities among the measured signals were investigated by using correlograms. Figures 24 ~ 29

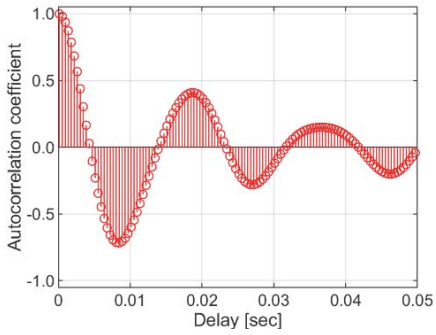

Figure 24. Run#1 KBL at the 1500/4 point.

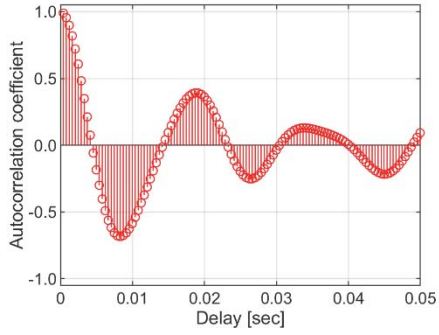

Figure 25. Run#2 severe knock in Cyl-1 at the 1500/4 point.

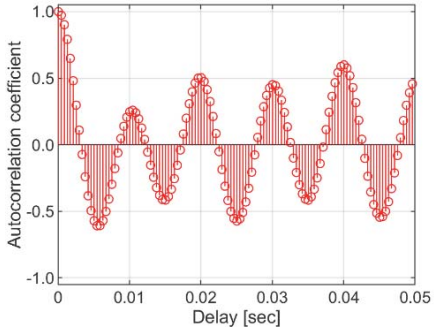

Figure 26. Run#4 KBL at the 1500/6 point.

show the correlograms of the low-frequency-band-filtered signals. The filter band was 10 ~ 100 Hz. This low-frequency band included the signal contents associated with normal combustion and engine revolution. For instance, the frequencies of normal combustion events were twice the frequencies corresponding to different engine speeds, for example, 50 Hz and 66.7 Hz for the engine speeds of 1,500 rev/min and 2,000 rev/min, respectively. All cases, regardless of whether KBL or severe knock, exhibited high

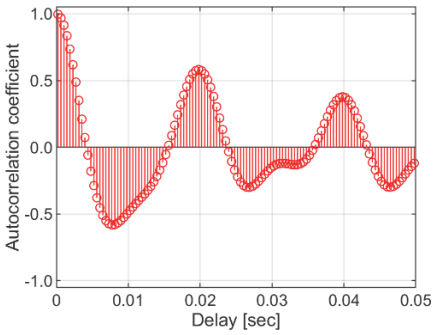

Figure 27. Run#5 Severe knock in Cyl-1 at the 1500/6 point.

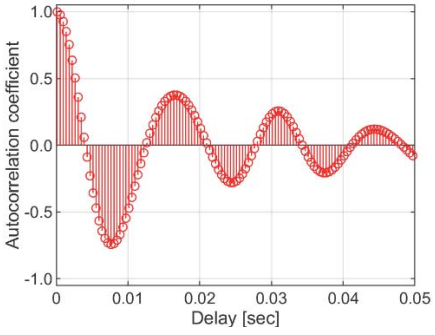

Figure 28. Run#7 KBL at the 2000/4 point.

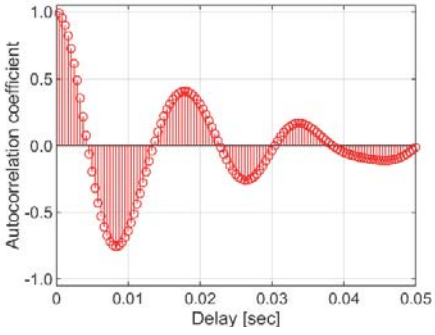

Figure 29. Run#8 Severe knock in Cyl-1 at the 2000/4 point.

similarity across signals. At the 1500/4 and 2000/4 points, the oscillations were stabler, and the discrepancy between the KBL and severe knock cases was smaller. This might be related to the weaker knocking at these two points, which required substantial spark timing advances of 15 and 12 CA, respectively. The 6-CA spark timing advance was sufficient for consistent and strong knocks at the 1500/6 point. The substantial discrepancy between the KBL and severe knock cases at the 1500/6 point can possibly be ascribed to the strong impacts of the high-intensity knocks due to normal combustion events.

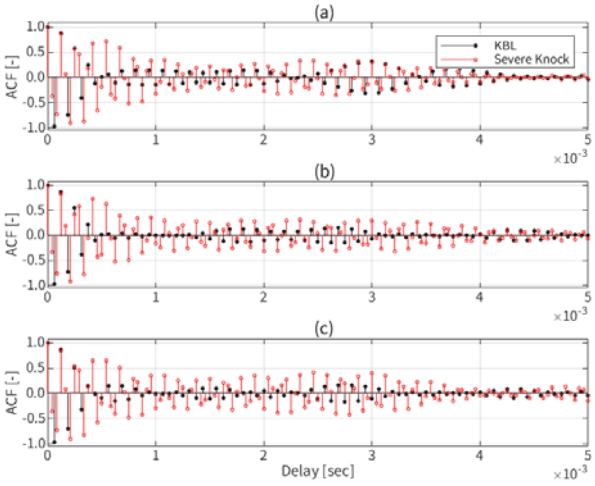

Figure 30. Autocorrelation functions of the KBL and severe knock cases at the (a) 1500/4; (b) 1500/6; (c) 2000/4 points.

Figure 30 shows the correlograms of the high-frequency-band-filtered KBL and severe knock cases. The frequency range of the bandpass filter was set to 7,000 ~ 8,000 Hz for the high-frequency components observed only in the severe knock cases, as shown in Figures 4 to 6. These auto-correlation functions (ACF) indicate that the severe knock cases exhibited stronger oscillation than the KBL cases, meaning that that the severe knock cases contained a stable and repetitive signal component in the 7,000 ~ 8,000 Hz band, while the KBL cases only contained the noise component in the same band.

The raw signal was processed by applying a bandpass filter to extract the knock sound component. Catch the knock sound from the original signal using the extracted sound component. However, it can identify only knocks of the same intensity, but not weaker or stronger knocks. The knock intensity was quantified based on the signal extracted post the bandpass filtering process.

4. CONCLUSION

In this study, the characteristics of the sound transmitted through a copper tube from the cylinder block was investigated with a high-compression-ratio, four-cylinder, spark-ignition engine. The analysis revealed similarities and consistent distinctions between the sounds recorded when the spark timing was set at the KBL and when it was significantly advanced. These consistent distinctions can be utilized to develop knock classification models. The major findings of this study are summarized below.

The FFT analysis showed that both types of sound signals, namely the KBL sound signals and the severe knock case sound signals, contained sound corresponding to the frequencies of engine speed and its multiples. The

signal components corresponding to the frequency of the engine speed were sufficiently consistent for use in engine speed determination.

Several features that distinguished severe knock from normal operation were obtained from the spectral analysis. The severe knock signal contained higher-frequency components at 7,000 ~ 8,000 Hz under all three operating conditions. In addition, the spectrogram indicated that it might be possible to distinguish a knocking cylinder from cylinders undergoing normal combustion.

According to the autocorrelation analysis, the severe knock cases were characterized by substantial high-frequency components in the 7,000 ~ 8,000 Hz band compared to those in the KBL cases under all operating conditions. Moreover, the autocorrelation of the high-frequency components provided effective features for knock cycle classification.

ACKNOWLEDGEMENT–This work was supported by the National Research Foundation of Korea (NRF) grant funded by the Korean government (MSIT) (No. 2019R1F1A1056540). Author would like to express special thanks to Korea Institute of Machinery and Materials and Hyundai Motors Company for technical supports.

REFERENCES

Abu-Qudais, M. (1996). Exhaust gas temperature for knock detection and control in spark ignition engine. *Energy Conversion and Management* **37**, **9**, 1383–1392.

Bennett, C., Dunne, J. F., Trimby, S. and Richardson, D. (2017). Engine cylinder pressure reconstruction using crank kinematics and recurrently-trained neural networks. *Mechanical Systems and Signal Processing*, **85**, 126–145.

Brunt, M. F., Pond, C. R. and Biundo, J. (1998). Gasoline engine knock analysis using cylinder pressure data. *SAE Trans.*, 1399–1412.

Cho, S., Song, C., Oh, S., Min, K., Ha, K. P. and Kim, B. S. (2018). An experimental study on the knock mitigation effect of coolant and thermal boundary temperatures in spark ignited engines. *SAE Paper No*. 2018-01-0213.

Ettefagh, M. M., Sadeghi, M. H., Pirouzpanah, V. and Tash, H. A. (2008). Knock detection in spark ignition engines by vibration analysis of cylinder block: A parametric modeling approach. *Mechanical Systems and Signal Processing* **22**, **6**, 1495–1514.

Glowacz, A. (2019). Acoustic fault analysis of three commutator motors. *Mechanical Systems and Signal Processing*, **133**, 106226.

Gryllias, K. C. and Antoniadis, I. A. (2013). Estimation of the instantaneous rotation speed using complex shifted Morlet wavelets. *Mechanical Systems and Signal Processing* **38**, **1**, 78–95.

Hamilton, L. J. and Cowart, J. S. (2008). The first wide-open throttle engine cycle: Transition into knock experiments with fast in-cylinder sampling. *Int. J. Engine Research* **9**, **2**, 97–109.

Kalghatgi, G. (2018). Knock onset, knock intensity, superknock and preignition in spark ignition engines. *Int. J. Engine Research* **19**, **1**, 7–20.

Lee, J. H., Hwang, S. H., Lim, J. S., Jeon, D. C. and Cho, Y. S. (1998). A new knock-detection method using cylinder pressure, block vibration and sound pressure signals from a SI engine. *SAE Trans.*, 1808–1819.

Leppard, W. R. (1982). Individual-cylinder knock occurence and intensity in multicylinder engines. *SAE Paper No*. 820074.

Liu, H., Wang, Z., Qi, Y., He, X., Wang, Y. and Wang, J. (2019). Experiment and simulation research on super-knock suppression for highly turbocharged gasoline engines using the fuel of methane. *Energy*, **182**, 511–519.

Liu, X., Randall, R. B. and Antoni, J. (2008). Blind separation of internal combustion engine vibration signals by a deflation method. *Mechanical Systems and Signal Processing* **22**, **5**, 1082–1091.

Maurya, R. K., Pal, D. D. and Agarwal, A. K. (2013). Digital signal processing of cylinder pressure data for combustion diagnostics of HCCI engine. *Mechanical Systems and Signal Processing* **36**, **1**, 95–109.

Nikula, R. P., Karioja, K., Pylvänäinen, M. and Leiviskä, K. (2020). Automation of low-speed bearing fault diagnosis based on autocorrelation of time domain features. *Mechanical Systems and Signal Processing*, **138**, 106572.

Novella, R., Pla, B., Bares, P. and Jiménez, I. (2022). Acoustic characterization of combustion chambers in reciprocating engines: An application for low knocking cycles recognition. *Int. J. Engine Research* **23**, **1**, 120–131.

Pachaud, C., Salvetat, R. and Fray, C. (1997). Crest factor and kurtosis contributions to identify defects inducing periodical impulsive forces. *Mechanical Systems and Signal Processing* **11**, **6**, 903–916.

Payri, F., Luján, J. M., Martín, J. and Abbad, A. (2010). Digital signal processing of in-cylinder pressure for combustion diagnosis of internal combustion engines. *Mechanical Systems and Signal Processing* **24**, **6**, 1767–1784.

Peyton Jones, J. C., Shayestehmanesh, S. and Frey, J. (2020). Parametric modelling of knock intensity data using a dual log-normal model. *Int. J. Engine Research* **21**, **6**, 1026–1036.

Peyton Jones, J. C., Spelina, J. M. and Frey, J. (2014). Optimizing knock thresholds for improved knock control. *Int. J. Engine Research* **15**, **1**, 123–132.

Pichler, K., Lughofer, E., Pichler, M., Buchegger, T., Klement, E. P. and Huschenbett, M. (2016). Fault detection in reciprocating compressor valves under varying load conditions. *Mechanical Systems and Signal Processing*, **70**, 104–119.

PowerLink (2020). Eddy current dynamometer working

principle. https://www.powerlinkpt.com/eddy-current-dynamometer-en/

Rafiee, J. and Tse, P. W. (2009). Use of autocorrelation of wavelet coefficients for fault diagnosis. *Mechanical Systems and Signal Processing* **23**, **5**, 1554–1572.

Su, W., Wang, F., Zhu, H., Zhang, Z. and Guo, Z. (2010). Rolling element bearing faults diagnosis based on optimal Morlet wavelet filter and autocorrelation enhancement. *Mechanical Systems and Signal Processing* **24**, **5**, 1458–1472.

Wang, Z., Liu, H. and Reitz, R. D. (2017). Knocking combustion in spark-ignition engines. *Progress in Energy and Combustion Science*, **61**, 78–112.

Wodecki, J., Kruczek, P., Bartkowiak, A., Zimroz, R. and Wyłomańska, A. (2019). Novel method of informative frequency band selection for vibration signal using Nonnegative Matrix Factorization of spectrogram matrix. *Mechanical Systems and Signal Processing*, **130**, 585–596.

Xu, J., Feng, Y., Chang, S. and Guo, T. (2020). Numerical and experimental study on knock sources in spark ignition engine with electromagnetic valve train. *Int. J. Automotive Technology* **21**, **6**, 1369–1378.

Yang, Z., Yan, W., Jin, L., Li, F. and Hou, Z. (2020). A novel feature representation method based on original waveforms for acoustic emission signals. *Mechanical Systems and Signal Processing*, **135**, 106365.

Yun, D. U. and Lee, S. K. (2017). Objective evaluation of the knocking sound of a diesel engine considering the temporal and frequency masking effect simultaneously. *J. Sound and Vibration*, **397**, 282–297.